A pre-injector upgrade for ISIS, including a medium energy beam transport line and an RF-driven H^- ion source

S. R. Lawrie, R. E. Abel, C. A. Cahill, D. C. Faircloth, J. H. Macgregor, S. Patel, T. C. de M. Sarmento, J. Speed, O. A. Tarvainen, M. O. Whitehead, T. Wood, and D. Zacek

Published version information

Citation: SR Lawrie et al. "A pre-injector upgrade for ISIS, including a medium energy beam transport line and an RF-driven H− ion source." Review of Scientific Instruments, vol. 90, no. 10 (2019): 103310. Is in proceedings of: 18th International Conference on Ion Sources (CIS'19), Lanzhou, China, 1-6 Sep 2019.

DOI: 10.1063/1.5127263

A pre-injector upgrade for ISIS, including a medium energy beam transport line and an RF-driven H^- ion source

Cite as: Rev. Sci. Instrum. **90**, 103310 (2019); https://doi.org/10.1063/1.5127263
Submitted: 10 September 2019 . Accepted: 02 October 2019 . Published Online: 18 October 2019

S. R. Lawrie, R. E. Abel, C. A. Cahill, D. C. Faircloth, J. H. Macgregor, S. Patel, T. C. de M. Sarmento, J. Speed, O. A. Tarvainen, M. O. Whitehead, T. Wood, and D. Zacek

Review of Scientific Instruments ARTICLE scitation.org/journal/rsi

A pre-injector upgrade for ISIS, including a medium energy beam transport line and an RF-driven H⁻ ion source

Cite as: Rev. Sci. Instrum. 90, 103310 (2019); doi: 10.1063/1.5127263
Submitted: 10 September 2019 • Accepted: 2 October 2019 •
Published Online: 18 October 2019

S. R. Lawrie,[a] R. E. Abel, C. A. Cahill, D. C. Faircloth, J. H. Macgregor, S. Patel, T. C. de M. Sarmento, J. Speed, O. A. Tarvainen, M. O. Whitehead, T. Wood, and D. Zacek

AFFILIATIONS

UK Research and Innovation, ISIS Pulsed Spallation Neutron and Muon Facility, Rutherford Appleton Laboratory, Oxfordshire, United Kingdom

Note: Contributed paper, published as part of the Proceedings of the 18th International Conference on Ion Sources, Lanzhou, China, September 2019.
[a]**Electronic mail:** scott.lawrie@stfc.ac.uk

ABSTRACT

The ISIS spallation neutron and muon facility is undergoing an upgrade to the negative hydrogen (H^-) linac preinjector with the addition of a medium-energy beam transport (MEBT) line. A fast electrostatic sweep chopper is included in the MEBT and will notch the linac bunch train at the synchrotron frequency. The MEBT and chopper will increase the beam transport efficiency significantly, reducing the output H^- current requirements from the ion source. As such, a long-lifetime, noncesiated, RF-driven, external-antenna H^- ion source based on the successful CERN Linac4 and SNS designs is constructed, which will improve facility uptime and reliability. This paper will highlight the latest developments on the MEBT before focusing on the RF ion source. The RF ion source must deliver 35 mA of H^- beam current in pulses 400 μs long at a 50 Hz repetition rate, with transverse normalized 4 rms emittances less than 1.2 π mm mrad. The beam current and emittance are within the reach of a noncesiated H^- source, whereas operating at relatively high duty cycles presents challenges in terms of thermal management, which this paper will address.

I. INTRODUCTION

The ISIS pulsed spallation facility[1] at the Rutherford Appleton Laboratory (RAL) has been delivering beams of neutrons and muons for materials characterization studies since 1984. The negative hydrogen (H^-) linac was upgraded in 2004 with the addition of a "preinjector" based around a 665 keV radio frequency quadrupole (RFQ).[2] A Penning-type cesium-enhanced surface-plasma ion source supplies the preinjector with around 55 mA of H^- beam current. Limitations in beam transport efficiency mean that over 50% of beam current is lost between the ion source and the synchrotron. Moreover, the Penning source lifetime is limited by material sputtering inside the plasma chamber, meaning that facility operations must be stopped every three weeks to replace the ion source.

To address these issues, the preinjector is upgraded with the installation of a medium energy beam transport (MEBT) line. The MEBT matches the divergent RFQ beam with the acceptance of the first drift tube linac (DTL) tank. With proper matching, beam transport efficiency of over 96% is expected between the RFQ and the synchrotron, compared to 70% simulated and measured at present. The improved transport will reduce the radioactivation of accelerator components and it lowers the output requirements of the H^- ion source.

II. MEDIUM ENERGY BEAM TRANSPORT

The MEBT consists primarily of eight electromagnetic quadrupoles and four quarter-wave resonator (QWR) rebunching cavities. Beam diagnostics include four extremely compact button-type beam position monitors (BPMs) based on those designed for the front end test stand (FETS)[3] and two beam current transformer toroids. Finally, a fast electrostatic sweep chopper is installed, which is based on the prototype tested on the vessel for extraction

and source plasma analyses (VESPA).[4] The chopper will notch the 202.5 MHz linac microbunch train at 1.3 MHz for clean injection into the synchrotron RF buckets. It will also remove the ripple at the start of the linac beam macropulse, while space-charge compensation in the low energy beam transport (LEBT) builds up over around 150 μs. Room was made upstream of the ion source to allow shifting of the present preinjector away from the DTL for insertion of a MEBT.[5] Figure 1 shows the close packing of beamline components required due to the difficulty in controlling the low energy beam under high space charge forces. As such, the entire MEBT lattice is just 1.8 m long. Individual components are constrained too tightly to replace easily in the event of a failure, so the MEBT is split into three "rafts" that can be removed quickly for component reassembly and alignment off-line. The chopper in raft 2 consists of two 160 mm long plates held at ±7.5 kV to deflect the beam onto a cooled tungsten dump. The dump position will be adjusted during commissioning to maximize chopping efficiency while minimizing beam collimation. Vacuum line valves are installed after rafts 1 and 3 to allow the RFQ and DTL tank 1 to remain under vacuum, while the chopper dump height is adjusted iteratively. The ion source and LEBT vacuum are isolated from the RFQ via another line valve at the input end of the RFQ.

III. MEBT IMPLICATIONS ON THE ION SOURCE

The ISIS linac delivers 26 mA, 240 μs macropulses routinely to the synchrotron (ring). At present, the ring operates with H^- charge exchange injection into 180° of phase. The RF amplitude is then increased and the phase length reduced to trap the beam into buckets. Around 3% of loss occurs during RF trapping, which contributes significantly to ring activation. The MEBT chopper will notch around 30% of the linac microbunches to facilitate direct injection into 120° phase buckets, thus removing all trapping losses. No activation will occur at the chopper due to the lower beam energy. To maintain the same integrated charge injected into the ring, the (chopped) linac beam pulse must increase to 35 mA and 300 μs. The matched beam from the MEBT improves linac transmission significantly, and, with a two-solenoid (LEBT) line coupled closely to the ion source, the total beam-loss from source to ring will be less than 7%. This means that the ion source needs to produce 38 mA to deliver the required beam, even with the inclusion of the chopper. Without the chopper, only 28 mA is needed from the source. These currents are within reach of a noncesiated volume-production RF-driven H^- ion source. The RF ion source will significantly have longer maintenance interval than the present Penning source and will have more operational flexibility.

IV. RF ION SOURCE

The RF ion source[6] is based on the designs using external RF antennas at CERN's linac4[7] and the ORNL's SNS.[8] Recent studies have shown that noncesiated RF ion sources with 7.5 mm outlet apertures can produce over 40 mA of beam current,[6] provided that no restriction occurs between the filter magnet and aperture.[9] Other than delivering the required beam current, the main objective for the RAL RF ion source is reliability. Every effort must be made to deliver an ion source that can last an entire user cycle or more (at least 60 days; aiming for one year), with minimal operator intervention. The major hurdles to overcome in the design to achieve high reliability are cooling and vacuum systems able to operate at 50 Hz: a significant increase over CERN's 0.8 Hz operation.

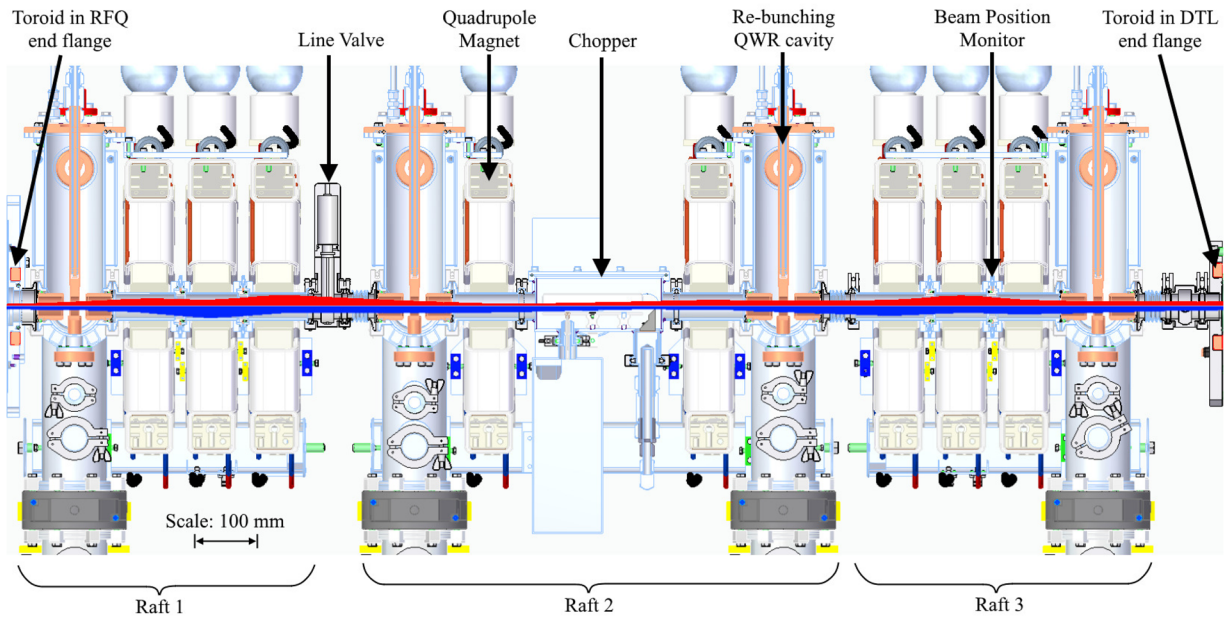

FIG. 1. Vertical (top, red) and horizontal (bottom, blue) cross sections of the MEBT with 5 rms beam envelope overlaid. Only one item of each component family is labeled for clarity. The beam is brought to a horizontal waist at the chopper dump.

A. Plasma chamber cooling jacket

The cooling system must cope with the maximum available power from the 2 MHz RF amplifier (100 kW and 1 ms long pulses at 50 Hz). Power is coupled into the plasma via an RF isolation transformer, a matching network of capacitors and inductors, and a 5½-turn solenoidal antenna mounted external to the plasma chamber. The chamber is a plain cylinder of aluminum nitride ceramic to maximize thermal conductivity. It has no machined grooves or other details which may crack under thermal load; however, it does have molybdenum rings brazed onto the ends to make reliable vacuum seals. The chamber is cooled by a "jacket" with cut grooves to direct cooling water onto the plasma loss lines of the octopole magnetic cusp field. The jacket must be nonconductive to prevent eddy-current losses from the external antenna. It must also be very compact to minimize the radial gap between antenna and plasma chamber, which would otherwise require higher input RF power. These limitations were mitigated by 3D-printing the jacket from a plastic material, with the benefit of allowing complex geometry, otherwise impossible to machine. The jacket's water flow channels were designed using the computational fluid dynamics (CFX) module of the ANSYS Workbench software. One quarter of the jacket was modeled, and cylindrical periodic boundary conditions were applied. Sixteen flow and return hose connections are needed for eight cooling channels, but CFX showed that these could be reduced to eight connections by splitting/combining channels with septa. Figure 2 shows the simulated water streamlines. Flow velocity is maintained below 3 ms^{-1} to minimize erosion.

Flow channels are oriented to minimize the amount of material in direct contact with plasma loss lines. Nevertheless, materials suitable for 3D-printing necessarily have relatively low melting points, so thorough off-line thermal testing was required. The full benefits of rapid prototyping were realized when nine iterations were required to ensure that the jacket (a) was leak-tight at full water pressure, both on the bulk printed body and at hydraulic o-ring seals, (b) could endure multiple assemblies and hose connections, (c) would not crack under repeated thermal cycling, and (d) would not erode or soften under full flow and heating power. The final design uses high temperature, glass-filled nylon-12 using the laser sintering technique. The jacket was run for a week at full flow, with eight 400 W heating elements applied. It was important to use the real ceramic plasma chamber as the heat application surface, as it has a similar thermal expansion coefficient to the plastic jacket, whereas a dummy aluminum chamber expanded too much and warped the jacket, causing small leaks around the o-ring seals. Dozens of thermal cycles were performed to simulate RF power being switched on/off: ensuring a robust, reliable design which matches CFX predictions.

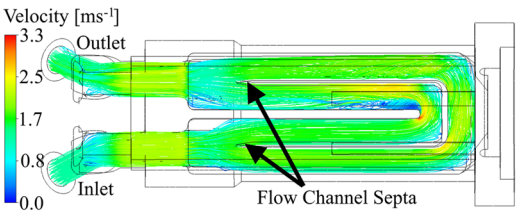

FIG. 2. Computational fluid dynamics simulation of the cooling jacket. Water streamlines colored by velocity.

B. Plasma electrode

The plasma electrode (PE) is biased electrically via aluminum nitride ceramic insulators to suppress coextracted electron emission. Significant power is absorbed by the PE, so local water cooling is applied, which also helps cool the nearby plasma chamber vacuum o-ring. 2D-axisymmetric ANSYS simulations show that good thermal contact conductance is critical to prevent PE over-heating. Therefore, high bolt torques and pyrolytic carbon gaskets will be used, which the present simulations and past measurements[10] show can reduce temperatures by several hundred degrees. The PE must operate below the onset of thermionic emission, as it faces the extraction electrode which would see intolerably high electron current loading from a hot PE. At full power and duty cycle, simulations show that the PE temperature can be maintained below 600 °C. A thermocouple probe monitors the local temperature to compare with simulation results.

Another important design consideration is the protection of the PE during fault conditions. During a high-voltage (HV) breakdown, the 10 kV extraction voltage will jump temporarily to the PE: far in excess of the PE power supply rating. As well as external protection circuitry, transient currents are shunted safely to ground across an internal spark gap. In addition, HV-rated kapton-insulated cable is used to connect the PE power. Figure 3 shows a 2D axisymmetric Vector Fields Opera electrostatic simulation of the optimized spark gap and protected insulator triple-junctions. Large HV gaps with no lines of sight to the plasma are employed to prevent insulator tracking. To avoid plasma poisoning, the only materials exposed to the plasma are molybdenum and aluminum nitride. However, a part near the PE has been designed to be replaced for testing H^- production enhancement from surface-effects using different materials.[11]

C. Electron dump cooling

The magnetic filter field and biased PE will be tuned to minimize the coextracted electron current. Nevertheless, 1–2 A of 10 keV electrons need to be removed safely at 50 Hz using SmCo deflector magnets. Following the work performed at CERN,[12] the

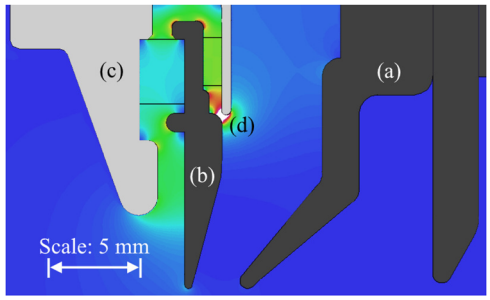

FIG. 3. Simulation of a high voltage fault condition whereby the extraction electrode (a) sparks to the plasma electrode (b), which then sparks immediately to ground (c) across a dedicated spark gap (d). Colored contours show electric field strength, with white exceeding the 10 MV m^{-1} vacuum breakdown limit.

electron dumping (edump) scheme was designed[6] to limit surface power density below 1 kW mm^{-2} with an e/H^- ratio of 50. Transient thermal simulations of a water-cooled tungsten edump with worst-case power and duty cycle show a peak temperature of 2000 °C, falling to 500 °C between pulses. Therefore, the tungsten will not melt, but evidence of local heating is expected after prolonged operation. Note that the highest temperatures are where the electron beam spot collides deep inside the edump. The rest of the electrode is much lower at around 60 °C, so thermionic emission is not a concern. The edump magnets are isolated thermally from the hot spot and will be far below SmCo's Curie temperature. Nevertheless, an electrically isolated fiber-optic thermocouple forms part of the safety interlock chain to protect the magnets, and the power and duty factor will be raised slowly during commissioning.

D. Vacuum vessel and low energy beam transport

To simplify the beam optics and reduce emittance growth, no einzel lens is used to match the extracted ion beam to the LEBT. Instead, the ion source is mounted as close as possible to the first LEBT solenoid for prompt focusing of the divergent H^- beam. The drawback of a small gap between the ion source and solenoid is reduced vacuum conductance. Molflow vacuum simulations were performed to achieve a good compromise between high pumping efficiency and compact beam transport. The vessel is a rectangular box welded from plates with critical alignment features machined postwelding. The tolerance stack leads to a 0.5 mm worst-case transverse offset of the ion source emission and extraction apertures relative to the nominal beam axis. With support braces welded inside the vessel, vacuum loading stress calculations show a worst case longitudinal deflection of 0.15 mm. Four 1100 l s^{-1} turbomolecular pumps are mounted on the side walls, which must remove 20 sccm of H_2 fed continuously into the ion source. Simulations show that the pumping speed is sufficient to maintain a pressure better than 8×10^{-5} mbar after beam extraction. This low pressure ensures less than 5% H^- stripping losses through collisions with residual gas molecules.

The vessel is supported by kinematic mounts on the beamline rails. The H^- ion beam is deflected a small amount by the edump magnets. Instead of correcting the beam with anti-dipole magnets[13] or adjustable ion source bellows,[14] the entire vessel is tilted relative to the LEBT. This is a nontrivial exercise because the ion source will be adjusted depending on the facility requirements. In addition, the space charge at extraction depends strongly on the coextracted electron current: as yet unknown. However, the beam perveance will be matched by adjusting the extraction voltage that affects the beam deflection angle from the edump. It is undesirable to adjust the vessel position for each ion source setting, so a nominal vessel setup is required. Comprehensive IBSimu[15] beam tracking studies were performed to find an optimum vessel tilt of 35 mrad and an offset of 5.0 mm relative to the LEBT beampipe. Figure 4 shows that the H^- beam is injected into the RFQ with a beam centroid displacement less than ±0.5 mm and ±10 mrad for all possible ion source outputs, with the nominal setting well centered in both transverse planes. Without the tilted vessel, the beam would enter the RFQ offset up to ±7 mm and ±40 mrad. Note that the centroid will be further perfected during operation using small electromagnetic steering dipoles embedded in the solenoid magnets. The tilted vessel is connected to the LEBT beampipe via a short bellows. The bellows is welded to the beampipe at an angle, so it is unstressed in its nominal position, allowing mechanical adjustment during alignment.

E. Assembly procedure

Figure 5 shows a side view of the RF ion source and the LEBT. Electrical bias is applied to the ion source via an insulator made from ertacetal copolymer. The insulator is re-entrant to the vessel but has sufficient radius for easy operator access inside. Accessibility and ease of removal are very beneficial for troubleshooting and quick replacement of components during both commissioning and long-term facility operation. Therefore, the ion source and its insulators can be assembled as an entire unit offline and craned onto the vacuum vessel. Alternatively, most parts of the ion source can be removed *in situ*. For example, without breaking vacuum, the cusp magnets can be changed between two styles: one of which has an adjustable filter field.[6] The 3D-printed cooling jacket can be replaced equally easily if necessary. Cables, optical fibers, and quick-connect hoses are arranged neatly toward

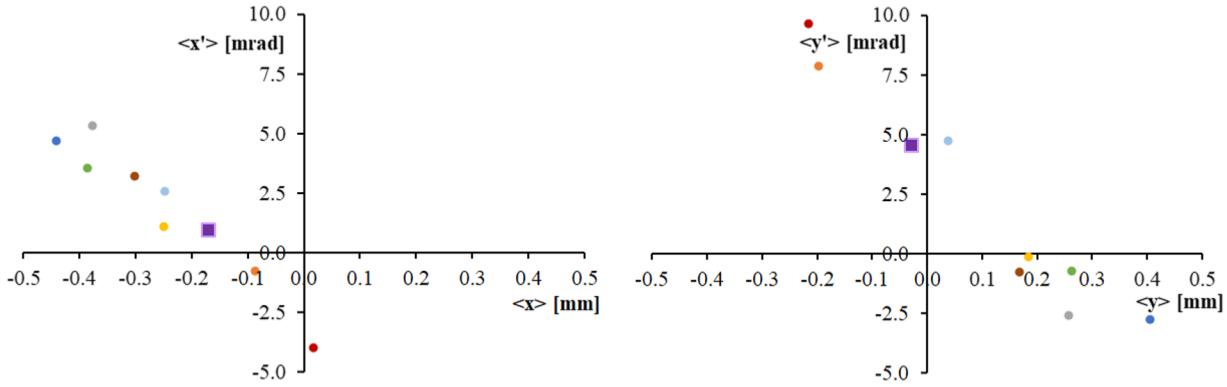

FIG. 4. Horizontal (left) and vertical (right) beam centroid position and angle at the RFQ entrance plane for nominal LEBT solenoid fields and ion source vessel tilt. The design beam is indicated by squares, with circles indicating a wide range of different ion source settings. In all cases, less than 3% beam loss occurs from the ion source to the RFQ, excluding residual gas H^- stripping losses.

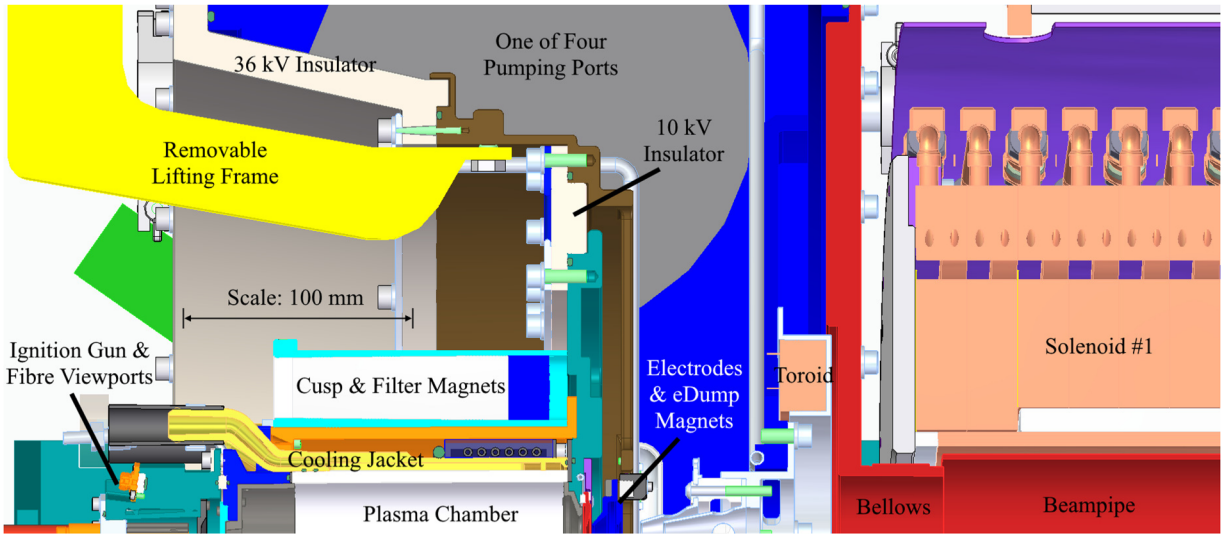

FIG. 5. Cross section of the RF source and first solenoid of the LEBT. The slight tilt between vacuum vessel and solenoid yoke can be discerned above the labeled bellows. The bottom edge of the image lies on the beam axis. The lifting frame is removed during ion source operation.

the center of the source. The vacuum system will be tested in stages; with various flanges blanked off as appropriate and particular attention paid to the plasma chamber vacuum seals. The plasma electrode defines the ion source datum, and the extraction electrode is aligned to it using a coaxial mandrel. The ground electrodes are aligned to the vessel and doweled in place. Finally, the overall vessel position is set relative to the LEBT using survey points. The close proximity of the vessel to the first solenoid is such that there is no room for a demountable vacuum sealing clamp near the bellows. Instead, a welded assembly (colored red in Fig. 5) consisting of the vessel flange, bellows, and beampipe is inserted into the solenoid and bolted outside the solenoid's radius. The RF matching box is supported on a wheeled frame. The RF isolation transformer is hidden away under the beamline rails. All design choices were made to facilitate the operator comfort as well as the desired beam output.

V. SUMMARY AND OUTLOOK

A new preinjector encompassing a noncesiated RF-driven ion source, LEBT, RFQ, and MEBT is assembled in a dedicated test area. The first RF ion source components will be delivered in late 2019 and beam commissioning is due in stages over 2020/21. The ion source and LEBT beam will be characterized fully using a movable diagnostics box including a toroid, Faraday cup, and Allison-type emittance scanners, before connecting to the RFQ and MEBT. The entire preinjector will then be soak-tested for one year to ensure that it is fit to run on the user facility. In parallel with assembly in the test area, the ISIS linac cabling and services will be modified such that the preinjector can be transferred efficiently in a short shut-down in 2023.

ACKNOWLEDGMENTS

Many thanks to CERN and SNS colleagues for their hospitality and invaluable advice in the ion source design phase.

REFERENCES

[1]J. Thomason, Nucl. Instrum. Methods Phys. Res., Sect. A **917**, 61 (2019).
[2]A. P. Letchford, C. P. Bailey, J. P. Duke, D. J. S. Findlay, and J. W. G. Thomason, in Proceedings of the European Particle Accelerator Conference, Paris, France, 2002, THPLE045.
[3]G. Boorman, S. M. Gibson, N. Rajaeifar, J. Pozimski, S. Jolly, S. R. Lawrie, A. P. Letchford, and J. D. Gale, in Proceedings of the International Beam Instrumentation Conference, Melbourne, Australia, 2015, TUPB073.
[4]S. R. Lawrie, D. C. Faircloth, J. D. Smith, T. M. Sarmento, M. O. Whitehead, T. Wood, M. Perkins, J. Macgregor, and R. Abel, Rev. Sci. Instrum. **89**, 052101 (2018).
[5]T. Wood, D. C. Faircloth, S. R. Lawrie, A. P. Letchford, M. O. Whitehead, T. Pike, and M. Perkins, Rev. Sci. Instrum. **87**, 02B121 (2016).
[6]O. Tarvainen, S. Lawrie, D. Faircloth, R. Abel, T. Sarmento, J. Macgregor, M. Whitehead, T. Wood, J. Lettry, D. Noll, J. Lallement, J. Angot, P. Sole, and T. Thuillier, AIP Conf. Proc. **2052**, 050005 (2018).
[7]J. Lettry, S. Bertolo, U. Fantz, R. Guida, K. Kapusniak, F. D. Lorenzo, C. Machado, C. Mastrostefano, T. Minea, M. O'Niel, H. Neupert, D. Noll, D. Steyaert, and N. Thaus, AIP Conf. Proc. **2052**, 050008 (2018).
[8]R. F. Welton, A. Aleksandrov, V. G. Dudnikov, B. X. Han, S. N. Murray, T. R. Pennisi, M. Piller, Y. Kang, M. Santana, and M. P. Stockli, AIP Conf. Proc. **1655**, 030002 (2015).
[9]T. Sarmento, S. Cousineau, D. Faircloth, B. Han, S. Lawrie, S. Murray, T. Pennisi, T. Sarmento, C. Stinson, M. Stockli, O. Tarvainen, and R. Welton, AIP Conf. Proc. (these proceedings).
[10]T. Rutter, D. Faircloth, D. Turner, and S. Lawrie, Rev. Sci. Instrum. **87**, 02B131 (2016).
[11]Y. An, B. Jung, and Y. S. Hwang, Rev. Sci. Instrum. **81**, 02A702 (2010).
[12]Ø. Midttun, T. Kalvas, M. Kronberger, J. Lettry, H. Pereira, and R. Scrivens, AIP Conf. Proc. **1515**, 481 (2013).
[13]A. Ueno, New J. Phys. **19**, 015004 (2017).
[14]S. K. Mukherjee, D. Cheng, M. A. Leitner, K. N. Leung, P. Luft, R. Gough, R. Keller, and M. D. Williams, in Proceedings of the Particle Accelerator Conference, New York, USA, 1999, WEA14.
[15]T. Kalvas, O. Tarvainen, T. Ropponen, O. Steczkiewicz, J. Ärje, and H. Clark, Rev. Sci. Instrum. **81**, 02B703 (2010).